NISTIR 6830

Strength and Ductility of Concrete Beams Reinforced with Carbon FRP and Steel

Dat Duthinh
Monica Starnes

U.S. DEPARTMENT OF COMMERCE
Technology Administration
Building and Fire Research Laboratory
National Institute of Standards
and Technology
Gaithersburg, MD 20899

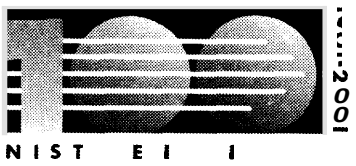

National Institute of Standards and Technology
Technology Administration
U.S. Department of Commerce

NISTIR 6830

Strength and Ductility of Concrete Beams Reinforced with Carbon FRP and Steel

Dat Duthinh
Monica Starnes

U.S. DEPARTMENT OF COMMERCE
Technology Administration
Building and Fire Research Laboratory
National Institute of Standards
and Technology
Gaithersburg, MD 20899

November 2001

U.S. DEPARTMENT OF COMMERCE
Donald L. Evans, Secretary

TECHNOLOGY ADMINISTRATION
Phillip J. Bond, Under Secretary
of Commerce for Technology

NATIONAL INSTITUTE OF STANDARDS
AND TECHNOLOGY
Karen H. Brown, Acting Director

ABSTRACT

Seven concrete beams reinforced internally with varying amounts of steel and externally with carbon fiber-reinforced polymer (FRP) laminates applied after the concrete had cracked under service loads were tested under four-point bending. Strains measured along the beam depth allowed computation of the beam curvature in the constant moment region. Results show that FRP is very effective for flexural strengthening. **As** the amount of steel increases, the additional. strength provided by the carbon FRP laminates decreases. Compared to a beam reinforced heavily with steel only, beams reinforced with both steel and carbon have adequate deformation capacity, in spite of their brittle mode of failure. Clamping or wrapping of the ends of the laminate enhances the capacity of adhesively bonded FRP anchorage. Design equations for anchorage, allowable stress, ductility, and amount of reinforcement are discussed.

Keywords: anchorage, beam, carbon fiber-reinforced polymers, ductility, flexure, FRP, reinforced concrete, repair, strengthening.

DISCLAIMER

Certain trade names and company products are mentioned in the text or identified in an illustration in order to adequately specify the experimental procedure and equipment used. In no case does such an identification imply recommendation or endorsement by the National Institute of Standards and Technology, nor does it imply that the products are necessarily the best available for the purpose.

Contents

Strength and Ductility of Concrete Beams Reinforced with Carbon FRP and Steel

1. Introduction and Review

The use of fiber-reinforced polymer (FRP) composites for the rehabilitation of beams and slabs started about 15 years ago with the pioneering research performed at the Swiss Federal Laboratories for Materials Testing and Research, or EMPA (Meier, 1987). Most of the work since then has focused on timber and reinforced concrete structures, although some steel structures have been renovated with FRP as well. The high material cost of FRP might be a deterrent to its use, but upon a closer look, FRP can be quite competitive. In addition to their resistance to corrosion, FRP have high ratios of strength and stiffness to density. The light weight of FRP provides considerable cost savings in terms of labor: a worker can handle the FRP material, whereas a crane would be required for its steel equivalent. FRP laminates and fabric come in great lengths, which can be cut to size in the field, as compared with welding of steel plates. FRP laminates or fabric are thin, light and flexible enough to be inserted behind pipes, electrical cables, etc., further facilitating installation. With heat curing, epoxy can reach its design strength in a matter of hours, resulting in rapid bonding of FRP to the structure and consequently, minimum disruption to its use.

The tensile strength of FRP can exceed 3000 MPa (compared to 400 MPa for reinforcing steel), and their stiffness ranges from slightly greater than that of steel for high-modulus carbon to about 1/3 that of steel for S-glass. FRP do not exhibit plastic yielding as steel does, however, and behave elastically up to an ultimate strain in the range of 1.5 % to 5 % (compared with a range of 15 % to 20 % for reinforcing steel). This brittle behavior must be accounted for in structural design.

Where FRP composites are used as external reinforcement in the rehabilitation of reinforced concrete (RC) beams and slabs, they increase the strength (ultimate limit state) and the stiffness (serviceability limit state) of the structure. Structural rehabilitation with FRP is thus motivated by requirements for earthquake strengthening, higher service loads, smaller deflections, or simply the need to complement deficient steel reinforcement. Care must be used to ensure that the concrete surface to which the strengthening is applied is sound, and the bonding between FRP and concrete is good. The increase in strength and stiffness is sometimes realized at the expense of a loss in ductility, or capacity of the structure to deflect inelastically while sustaining a load close to its capacity.

A number of issues still impede the routine use of FRP as a structural strengthening material. Chief among them is the absence of a long record of use, causing concern about durability with potential users. Another concern is fire resistance, especially as rehabilitation with FRP expands from highway bridges to buildings. The absence of standards is also an impediment, but this is being remedied through the efforts of various individuals and organizations such as the American Concrete Institute. At the time of this writing, ACI Committee 440 has produced a draft *"Guide for the Design and Construction of Externally Bonded FRP Systems for Strengthening Concrete Structures"*. The Canadian Standards Association (2000), the

(European) Federation Internationale du Beton (2001), the (British) Concrete Society (2001), and the Japan Building Disaster Prevention Association (1999) have published similar documents.

Recently, Naaman et al. (2001, 1999) reported on a series of tests of RC beams strengthened in flexure or shear with carbon FRP and loaded under static or cyclic loads, at room or low temperatures. The test parameters included the amounts of reinforcing steel and FRP, concrete cover thickness and condition (with repair mortar used to simulate damaged concrete), and anchorage configurations. The work includes a Substantial review of the literature, which is updated here. The authors found that, for a given reinforcement ratio, the ultimate load capacity increased but the ultimate deflection, and therefore ductility, decreased with the strengthening level. The three beams with various anchorage conditions (extended length, perpendicular wrap or normal condition, i.e., with no extra effort to enhance anchorage) had the same ultimate load and deflection. Naaman et al. recommended limiting the increase in strength due to FRP to 20 % of the nominal flexural strength of the beam with the maximum steel reinforcement ratio allowed by the ACI 318 Code (American Concrete Institute, 1999).

1.1 Ductility

Ductility is a desirable structural property because it allows stress redistribution and provides warning of impending failure. Steel-reinforced concrete beams are under-reinforced by design, so that failure is initiated by yielding of the steel reinforcement, followed, after considerable deformation at no substantial loss of load carrying capacity, by concrete crushing and ultimate failure. This mode of failure is ductile and is guaranteed by designing the tensile reinforcement ratio to be substantially below (ACI 318 requires at least 25 % below) the balanced ratio, which is the ratio at which steel yielding and concrete crushing occur simultaneously. The reinforcement ratio thus provides a metric for ductility, and the ductility corresponding to the maximum allowable steel reinforcement ratio provides a measure of the minimum acceptable ductility.

The design of FRP external reinforcement for flexure is fairly rational and straightforward. It is based on Bernoulli's hypothesis of strain compatibility that plane sections remain plane, which requires perfect bonding between FRP and concrete, and the ability of the concrete to transfer stresses to the FRP laminate by shear. In a beam reinforced internally with steel and externally with FRP, there is usually substantial reserve capacity at steel yielding. After the steel reinforcement yields, the beam can still carry increasing loads, albeit at a lower rate (with respect to deflections) than prior to steel yielding, and the FRP maintains elastic behavior until failure occurs suddenly. Failure is precipitated by FRP debonding, rupturing, or concrete crushing. All of these modes of failure are brittle, i.e., load capacity is reached with little inelastic deformation.

The FIB (Federation Internationale du Beton) Bulletin ***FRP Reinforcement for Concrete Structures*** (2001) notes that, if the design is governed by the Serviceability Limit State, the amount of FRP provided to the structure may be considerably higher than what is needed for the Ultimate Limit State. In this case, it may be difficult to fulfill ductility requirements (Triantafillou et al. 2001).

The Canadian Highway Bridge Design Code (CHBDC, 2000), based on the work of Jaeger et al. (1997), assesses the ductility of FRP-strengthened sections with a performance factor equal to $\frac{M_u \phi_u}{M_{.001} \phi_{.001}}$, where M and ϕ are the beam moment and curvature and the subscripts u refer to the ultimate state, and 0.001 to the service state that corresponds to a concrete maximum compressive strain of 0.001. This performance factor must be greater than 4 for rectangular sections and greater than 6 for T-sections.

1.2 Anchorage

Debonding or anchorage failure of the FRP occurs in the majority of tests of beams strengthened for flexure (64 % according to a survey by Bonacci, 1996). In only 22 % of the tests surveyed, rupture of the FRP was achieved, with the rest of the beams failing in shear or compression. It is not unusual for a carbon FRP laminate to debond at strains about half of its ultimate strain, oftentimes due to weakness in the concrete substrate rather than in the epoxy. In order to achieve. a more efficient use of this expensive material, more research on anchorage, development length and bond stress distribution is called for, e.g., research on the use of clamps, anchor bolts, U-shaped straps or wraps near the laminate ends, and staggered cut-off of multi-layer laminates.

Smith and Teng (2001) reviewed existing models of debonding of the laminate end, either by separation of the concrete cover or interfacial debonding of the FRP laminate from the concrete. They found that, with only one exception, the models developed for steel-plated concrete beams gave better predictions than those developed especially for FRP-laminated concrete beams. On the other hand, Aprile et al. (2001) showed that RC beams strengthened with elasto-plastic steel plates or elastic-brittle carbon laminates exhibit rather different behaviors. The steel plate yields before the internal reinforcement does, whereas no such behavior exists for the carbon laminate. Also, bond stress distribution in the shear span is different for steel plates than for carbon laminates.

According to Neubauer and Rostasy's work (1997, also in Rostasy, 1998, and Jensen et al. 1999), which has been adopted by the (British) Concrete Society in its *Design Guidance For Strengthening Concrete Structures Using Fibre Composite Materials* (2000), and the German Institute of Construction Technology (1997), the capacity of adhesively bonded anchorage is:

$$\frac{T_{\max}}{\mathrm{N}} = 0.5\, k\, \frac{w}{\mathrm{mm}} \sqrt{\frac{E_L}{\mathrm{MPa}} \frac{t}{\mathrm{mm}} \frac{f_t}{\mathrm{MPa}}} \qquad (1)$$

where $k = 1.06 \sqrt{\frac{2 - w/b}{1 + w/400}} \geq 1.0$ is a factor that accounts for the relative width w of the laminate and b of the concrete member, E_L is the modulus of elasticity, t the thickness of the laminate, $\frac{f_t}{\mathrm{MPa}} = 0.18 \left(\frac{f_{cube}}{\mathrm{MPa}} \right)^{2/3}$ is the concrete surface pull-off strength, and f_{cube} the concrete cube compressive strength. The anchorage length needed to achieve this anchorage capacity is:

$$\frac{l_{\max}}{\mathrm{mm}} = 0.7 \sqrt{\frac{E_L}{\mathrm{MPa}} \frac{t}{\mathrm{mm}} \frac{\mathrm{MPa}}{f_t}} \qquad (2)$$

The formulas above only apply for $1.5\,\text{MPa} \le f_t \le 3.0\,\text{MPa}$. An anchorage length longer than l_{max} does not increase the ultimate bond force above T_{max}. Application of these formulas to the beams used in this study is presented in a later section.

An alternative criterion recommended by the Concrete Society (2000) to prevent premature peeling failure is to limit the longitudinal shear stress between the FRP and the concrete substrate to 0.8 MPa, a value based on steel plate bonding. The longitudinal shear stress should be checked at the plate ends, where the shear force acting on the strengthened portion of the member will be at its greatest, and at the location in the span where the steel reinforcement first yields. Designers should also keep in mind that debonding of the laminate usually starts where there is significant shearing displacement across diagonal or transverse cracks (Swamy and Mukhopadhyaya, 1999).

2. Approach

The issues addressed by the study reported in this paper are:

1. What is the flexural strength enhancement provided by FRP laminates, and is this enhancement predictable?
2. How ductile is the flexural behavior of concrete beams reinforced with steel and FRP?
3. How effective is clamping or wrapping of the FRP laminate in enhancing anchorage?

2.1 Beam Design

To address these issues, a series of seven beams was tested. All beams had nominal dimensions of 150 mm width *x* 460 mm height *x* 2950 mm length, but the amount of flexural reinforcement, both steel and carbon FRP, varied. In Table 1, the beam number refers to the U.S. size of the flexural steel reinforcement, e.g., beam 5 contains two #5 (16 mm) bars. Beam 9, with no carbon FRP, was a reference beam, and beam 10, with the maximum flexural steel ratio allowed by **ACI** 318, was not fabricated but was used in calculations. The nominal concrete strength was 40 MPa and the nominal yield strength of the steel reinforcement was 415 MPa.

Table 1: Beam Properties

Beam	b	h	d	f_c	A_s	ρ_s / ρ_b	f_y	A_L	M_R/M_V	Anchor
	mm	mm	mm	MPa	mm^2	%	MPa	mm^2	%	
4a	152	460	415	42.3	253	11	430	60.9	68	clamp
4b	152	457	413	42.7	253	11	433	121.8	52	d.wrap*
5	156	460	414	42.3	400	18	506	60.9	34	wrap
6	152	457	410	41.5	568	25	453	60.9	36	clamp
7 N	152	457	408	41.9	774	35	469	60.9	33	clamp
8 N	157	460	406	42.0	1019	46	464	60.9	31	wrap
9	159	457	405	42.8	1290	58	453	0	---	---
10+	152	457	403	42.8	1639	73	453	0	---	---

+ not fabricated, contains maximum permitted steel ratio

* diagonal wrap

Shear and bearing steel reinforcements were provided in ample amount to ensure that failure occurred by flexure only. The shear reinforcement consisted of #3 bars (10 mm) in closed horizontal loops spaced at 120 mm and #3 vertical stirrups spaced at 100 mm and terminated by 135° hooks (Figs. 1 and 2). Bearing reinforcement in the form of #3 loops were placed under the bearing plates (Fig. 1).

2.2 Test Set-Up

The beams were cast with the compression side up but were tested under four-point loading with the tension side up for ease of application of the FRP laminate (Fig. 1). An array of eight LVDTs (linear variable differential transformers), 100 mm in gage length, spaced evenly over the sides of the beam, parallel to its axis, and supplemented with strain gages on the concrete, steel and carbon FRP laminate measured the strain profile of the beam at midspan (Figs. 1 and 2). Three additional LVDTs measured the deflections of the beam under its supports and at midspan.

2.3 External Strengthening

In most cases, strengthening was performed with the application of carbon FRP laminates shortly after the first flexural cracks appear, at about 1/3 of the calculated ultimate moment of the (virgin) beam reinforced with steel only. For beams 4a and 4b, the FRP laminate was applied at a higher ratio of the ultimate moment of the virgin beam ($M_R/M_V = 68$ % and 52 % respectively), as might occur in lightly reinforced beams (Table 1). Load was maintained during the application of the FRP laminate and curing of the adhesive.

External strengthening followed the procedures recommended by the manufacturer. The concrete surface was roughened with a scaler to expose the aggregate, then cleaned by air jet and acetone to rid it of loose particles and dust. The adhering face of the carbon laminate was also cleaned with acetone. **A** two-part adhesive (black and white) was mixed in 3:1 proportion, until the color was a uniform gray, then applied with a special tool to the concrete surface to a width of 52 mm (104 mm for beam 4b) and a thickness of 1.5 mm. The adhesive was also applied to the laminate to the same thickness. The laminate was then placed on the concrete, epoxy to epoxy, and a rubber roller was used to properly seat the laminate by exerting enough pressure so the epoxy was forced out on both sides of the laminate and the adhesive line did not exceed 3 mm in thickness. The carbon laminate was then covered with a heating tape and left' undisturbed to cure for 24 hours. The heating tape temperature was warm to the touch and estimated to be about 50° C.

Slant-shear tests: To measure the bond strength of the adhesive, three slant-shear tests similar to ASTM test method C 882 were performed. In each test, a concrete cylinder 100 mm in diameter and 200 mm in height was sawed in half along a 30° angle to its axis. A strip of carbon FRP 140 mm x 50 mm was bonded to both halves following the manufacturer's recommended procedures described above, with the rest of the matching surfaces of the concrete cylinder halves covered with Teflon@ape. Compression of the test specimens subjected the adhesive to a shear force and a normal compressive force in the ratio of cosine 30" to sine 30°. Failure occurred in the concrete and not at the interface of concrete with adhesive. Results showed that

one day dry cure was sufficient to develop the bond strength of the adhesive, calculated as the ratio of the shear force to the bonded area (Table 3).

Table 2 Properties of carbon laminate

	f_{Lu}	ε_{Lu}	E_L	t	w	% fiber
	MPa	%	GPa	mm	mm	(volume)
Manufacturer	2400	1.9	155	1.2	50	> 68
Test 1	3060	1.89	162			
Test 2	3020	2.20	156*			

*linear up to a stress of 2500 MPa and a strain of 1.60 %.

Table 3 Properties of adhesive (from manufacturer, except where noted)

Bond strength (MPa)					Tensile strength	Shear strength	Ultimate strain
Concrete-concrete		Carbon-concrete (measured here)					
2 day dry cure	14 day moist cure	1 day dry cure	2 day dry cure	7 day dry cure	7 day (MPa)	14 day (MPa)	7 day (%)
22.0	21.3	20.1	17.4	21.0	24.8	24.8	1

Tensile strength	Ultimate strain	Thickness	Modulus of elasticity	Strength/width	Mass/area
960 MPa	1.33 %	0.33 mm	73.1 GPa	3 16 kN/m/layer	230 g/m^2

Table 5 Properties of impregnating resin (from manufacturer)

Tensile strength	Ultimate strain
30 MPa	1.5 %

Tensile tests: Two tensile specimens of the carbon FRP laminate 50 mm in width by 508 mm in total length were tested to failure. The ends of the specimens were 140 mm long and consisted of three layers of the laminate bonded together with the same adhesive as the one used for bonding to concrete. The adhesive thickness was 3 mm in specimen 1, and 1.5 mm in specimen 2. To enhance friction, four layers of emery cloth were inserted between each face of the specimen and the machine grips. Failure occurred suddenly in the middle, single thickness region. Specimen 1 behaved linearly up to failure, whereas specimen 2 exhibited some non-linearity toward the end of the test (Table 2). The testing machine recorded directly the tensile load and deformation, from which stress and strain were obtained. The modulus of elasticity was obtained by fitting a straight line over the linear portion of the stress-strain curve, which was most of the curve for specimen 1 and up to 2500 MPa for specimen 2. Since only two tensile tests were conducted, and the FRP laminates never failed in tension in the beam tests, the manufacturer's material properties were used for analysis.

2.4 Anchorage

The carbon laminate was 2440 mm long and covered the middle of the tension face of the beams, leaving gaps of 50 mm between it and the load bearing plate at each end. For beams 4a, **6** and 7N, clamps torqued to 400 N·m applied compressive forces estimated (from thread geometry and estimated friction coefficient) to be between 15 kN and 25 kN onto the end 200 mm of the laminate (Fig. **3).**

For the other beams, carbon fiber fabric wraps 200 mm in width, placed on both sides of the beam, were used to anchor the carbon laminate. For beam 4b, six layers of wrap were placed diagonally at each end. For beams 5 and 8N, two layers of wrap were used, diagonally at one end, and transversely at the other (Fig. 4). The wrap application followed this procedure:

1. Round-off concrete beam edges to a radius of 15 mm;
2. Smooth out epoxy at edges of laminate to ensure that epoxy thickness decreased from **3** mm to 0 at a gradual slope;
3. Clean concrete surface;
4. Apply impregnating resin onto concrete surface with a paint brush;
5. Place wrap fabric onto resin with gloved hands and smooth out;
6. Work out any irregularities or air pockets with a plastic laminating roller; let the resin squeeze out between the rovings of the fabric;
7. Apply additional resin and repeat if additional layers are required;
8. Add a final layer of resin onto the exposed layer.

3. Theoretical Prediction

A computer program was developed to calculate the moment and curvature of rectangular concrete beams under uniform moment, with internal steel and external carbon FRP reinforcements. Fig. 5 shows the assumed model used in the following steps:

1. Assume a value of compression depth c ;
2. Assume a value of concrete compressive strain at extreme fiber ε_{cM} ;
3. Calculate beam curvature: $\frac{1}{r} = \frac{\varepsilon_{cM}}{c}$;
4. Compute steel strain: $\varepsilon_s = \frac{d-c}{r}$;
5. Determine strain in extreme tension fiber: $\varepsilon_t = \frac{h-c}{r}$;
6. Estimate laminate strain: $\varepsilon_L = \varepsilon_h - \varepsilon_i$, where the tensile strain on the concrete surface at FRP laminate application, ε_i , is calculated from the applied load. Since the FRP laminate is applied with the beam under an initial load, the FRP strain is less than that based on the strain profile obtained from steel and concrete;
7. Compute concrete compressive strain as a function of distance from neutral axis: $\varepsilon_c = \frac{\varepsilon_{cM}}{c} y$,
8. Calculate force in steel: $F_s = A_s E_s \varepsilon_s \le A_s f_y$;

9. Estimate laminate force: $F_L = 0$ if $\varepsilon_L \le 0$ or $\varepsilon_c \ge \varepsilon_{Lu}$; $F_L = A_L E_L \varepsilon_c$ otherwise;

10 Determine concrete stress based on Hognestad's parabola: $\frac{\sigma_c}{f_c} = 2\frac{\varepsilon_c}{\varepsilon_0} - \left(\frac{\varepsilon_c}{\varepsilon_0}\right)^2$

11 Calculate concrete force by integration of stresses: $F_c = b f_c \left(\frac{\varepsilon_{cM} c}{\varepsilon_0} - \frac{\varepsilon_{cM}^2 c}{3\varepsilon_0^2}\right)$;

12. Locate center of concrete force (from concrete face): $a = \frac{c(4\varepsilon_0 - \varepsilon_{cM})}{4(3\varepsilon_0 - \varepsilon_{cM})}$;

13. Check force equilibrium: $F_c = F_s + F_L$?
    if no, return to step 2 and assume another value of ε_{cM};
14. If yes, compute moment: $M = F_s(d-a) + F_L(h-a)$;
15. Check for concrete crushing: $\varepsilon_{cM} \ge \varepsilon_{cu}$?
    if yes, beam has failed. If no, return to step 1 and assume another value of c.

The model predicts that all the beams tested would fail by concrete crushing, including beam 4a, which would come close to achieving FRP rupture. The model needs further improvement to incorporate debonding or anchorage failure. In addition, the ultimate moment and curvature of under-reinforced steel RC beams were calculated by the current ACI 318 (1999) method. The following equations, based on the rectangular stress block, were used:

$(0.85 f_c)(0.75c)b = A_s f_y$

$M_u = A_s f_y (d - 0.75 \sim 12)$

$\phi_u = \varepsilon_{cu} / c$

The concrete strength f_c was estimated from linear regression of results of compressive tests performed within a day of the beam tests (Fig. 6).

4. Results

Strains obtained at midspan with LVDTs and strain gages allowed the calculation of the beam curvature and the tensile strain on the concrete surface when the laminate was applied (from linear extrapolation). This strain value is added to the strain of the laminate measured by the strain gage to obtain a "modified" strain. If there is no slip between laminate and concrete, the modified laminate strain would fall on a straight line with the other strains measured at midspan. In general, but not in all cases, the measurements showed a roughly linear distribution, implying that plane sections remained plane and there was no slip of the laminate. Straight lines were fit to the strain profiles, and the slopes of these lines gave the curvatures.

The slender RC beams behaved in expected fashion under flexural loading. **As** loads increased, flexural cracks increased in number, width and depth. Shear cracks and flexural-shear cracks also appeared, propagating diagonally from the loads to the supports. The widest cracks, and oftentimes the ones that proved critical, started as flexural cracks opposite the loads, then propagated vertically over the entire depth of the beam due to a combination of flexure and vertical shear. There was considerable vertical shearing displacement at these cracks, causing the laminate to start debonding where it intersected the cracks (Beams 4b, 5, 7, 9).

Beam 4a (clamped): Failure was initiated by debonding of the carbon FRP laminate, which slipped 12 mm at one end. Examination of the failure surface after the load had been removed showed shear failure in the concrete substrate, with the adhesive and the laminate remaining intact. Shortly after debonding failure of the laminate, a horizontal shear failure plane also appeared at the level of the steel reinforcement. No sign of concrete crushing was observed.

As shown in Fig. 7, the agreement between experimental data and theoretical prediction is close for moment-curvature, but not for ultimate strength. The theoretical model ignores concrete in tension, and consequently is less stiff than the measurements at low values of moment, before concrete cracks in tension. The model also does not predict debonding failure, and therefore allows the carbon to increase in strain up to 1.86 %, close to its rupture strain, at which point concrete crushes. Had the anchorage held, this beam would be balanced in terms of combined steel and carbon tensile reinforcements versus concrete (i.e., FRP ruptures at the same time as concrete crushes, with steel having yielded previously). From the linear strain profile and the close agreement between measured and calculated moment-curvature, there appears to be strain compatibility of the carbon laminate with the concrete up to ultimate and sudden debonding.

Beam 4b (wrapped): Failure was due to concrete crushing. Wide 45° shear cracks were observed, but there was neither anchorage failure nor debonding. **As** shown in Fig. 10, the model was less stiff than the experiment, but predicted the ultimate strength and mode of failure well (152 kN·m vs. 151 kN·m measured, by concrete crushing). **As** shown in Fig. 11, the measured laminate strain was less than strain compatibility would require, thus indicating some slip between concrete and laminate, despite the lack of supporting visual evidence.

Beam 5 (wrapped): Wide flexure-shear cracks extended vertically above the load point at one end. The transverse wrap at the other end ruptured at one edge of the beam, causing the FRP laminate to debond abruptly (Fig. 28). There was no evidence of concrete crushing. The moment-curvature plot exhibited some drift in curvature while the FRP was curing (Fig. 13). The ultimate state was also not well predicted because of debonding of the FRP laminate. **As** in beam 4b, strain compatibility between concrete and carbon was less than perfect (Figs. 14 and 15).

Beam 6 (clamped): **At** midspan, on the compressive face, concrete spalled and showed severe distress towards the end of the test. The carbon FRP laminate then failed abruptly and showed evidence of interlaminar slip (about 12 mm) within the thickness of the laminate itself when clamps were removed. Wide vertical cracks extended over the depth of the beam above the load points, and a horizontal crack covered the plane of steel reinforcement (Fig. 29). When the failed beam was removed from the test machine by lifting it at its ends, these three major cracks connected and the central portion of the beam, rectangular in shape, fell off.

As shown in Fig. **16** and prior to steel yielding, model and experiment agreed well. Beyond steel yielding, however, the model was less stiff than the measurements, and did not capture the interlaminar slip, which began at a laminate strain of 0.78 %, and caused the load to level and drop gradually before sudden failure at a laminate strain of 1.25 %. Fig. 17 shows that the strain distribution is linear over the beam depth, and Fig. 18 shows that the predicted compression depth agrees better with experimental measurements before steel yielding than after.

Beam 7N (clamped): Failure was due to concrete crushing. In addition, two wide cracks occurred above the load points, one propagating vertically, the other diagonally and connecting to the crushing zone. Tapping with a coin showed some evidence of debond of the carbon laminate opposite the load points, but there was neither complete debond (within the epoxy or the concrete substrate) nor delamination (within the FRP laminate). Unfortunately, an electric power failure at just about the time the steel reinforcement was beginning to yield caused the subsequent data to be questionable, in spite of various safety measures and valiant recovery efforts. Prior to the incident, model and experiment agreed reasonably well (Figs. 19, 20, and 21).

Table 6a, b: Results

Beam	M_V kN·m	M_u kN·m	M_u / M_V	ε_{LM} 10^{-3}	$\varepsilon_{LM} / \varepsilon_{Lu}$	ϕ_V km^{-1}	ϕ_u km^{-1}	ϕ_u / ϕ_{Vb}	M_{001} kN·m	$\phi_{.001}$ km^{-1}	$M_u \phi_u / M_{.001} \phi_{.001}$
4a	44.0	93.5	2.13	10.07	0.53	113	30.6	1.75	63.8	14.6	3.1
4b	45.0	151	3.36	9.88	0.52	111	32.7	1.86	76.4	12.1	5.3
5	80.1	117	1.46	6.62	0.35	62.2	25.0	1.43	80.1	10.7	3.4
6	99.2	148	1.49	7.80	0.41	46.9	26.9	1.54	115	11.7	3.0
7 N	136	179*	1.32	6.23"	0.33	33.6	20.3	1.69	105	7.69	4.5
8 N	172	204	1.19	6.10	0.32	26.7	25.3	1.45	138	8.09	4.6
9	207	215	1.04			22.2	19.7	1.13	140	8.13	3.7
10	252*					17.5"		1.00	---	---	

Beam	Failure Mode	Notes	ε_L (10^{-3})	ε_i (10^{-3})		M (kN·m)		ϕ (km^{-1})	
				tests	theory	tests	theory	tests	theory
4a	debond	Ultimate (test)	10.07	1.33	1.16	93.5	84.5	30.6	28.0
		Ultimate (theory)	18.60				119		49.2
4b	crush	Ultimate (test)	9.88	1.31	1.17	151	123	32.7	28.6
		Ultimate (theory)	13.50				152		38.4
5	debond	Ultimate (test)	6.62	1.64	0.82	117	104	25.0	19.6
		Ultimate (theory)	15.10				139		41.1
6	slip	Ultimate plateau	7.80	0.96	0.97	148	130	24.6	23.5
		(test)	8.49			148	133	26.9	25.3
		Ultimate (theory)	12.90				151		36.6
7N	crush	Ultimate (test)	6.23	1.21	0.92	217	179	20.3	29.5
		Power failure	2.03						
		Steel yields	2.80						
8N	crush	Ultimate (test)	6.10	1.66					
		Ultimate (theory)	7.36						

Beam 8N (wrapped): Failure was due to concrete crushing. The wraps held, although concrete diagonal shear cracks were visible underneath. The critical crack started out as flexural crack, opposite one of the load points, then propagated at 45° towards midspan where it joined with the concrete crushing zone. The carbon FRP laminate debonded locally at its intersections with the

critical crack, but there was no overall debond. **As** shown in Fig. 22, the computer model and the experimental results agreed well over the entire range (predicted ultimate moment of 201 kN·m at a curvature of 26 km^{-1} vs. 204 kN·m and 25 km^{-1} measured). The ultimate laminate strain, however, was calculated to be 0.703 % vs. 0.610 % measured, although there was no evidence of slip in the laminate as shown in Fig. 23.

Beam 9 (no carbon): Failure was due to concrete crushing. In addition, two wide cracks occurred above the load points, one propagating vertically, the other diagonally and connecting to the crushing zone. **As** shown in Fig. 25, the agreement between model and experiment for this steel RC beam was reasonable (calculated ultimate moment of 207 kN·m at a curvature of 22 km^{-1} vs. 215 kN·m measured and an ultimate curvature between 19 km^{-1}, at the peak load, and 28 km^{-1} at failure). The difference in stiffness prior to steel yielding, here and in other cases noted above, may be due to errors in strain profile measurements, as shown, for example, in Fig. 26.

Results are summarized in Table 6, Figs. 30-32, and discussed below. Table 6b compares theory and experiments for various remarkable values of laminate strains, beam moment and curvature. These values include the theoretical ultimate states and the experimental ones.

Strengthening: The application of carbon FRP laminates is very effective for flexural strengthening of reinforced concrete beams, provided proper anchorage of the laminate is ensured. In one case (beam 4b), the strengthened beam was 3.33 times stronger than the original beam (Fig. 30). **As** the amount of steel reinforcement increases, the additional strength provided by the carbon FRP external reinforcement decreases. The same amount of FRP reinforcement more than doubled the flexural strength of a lightly reinforced beam (11 % of balanced ratio), but only increased by 19% the strength of a moderately reinforced beam (46 % of balanced ratio).

FRP strain limit: An informal proposal circulated in ACI Committee 440 (FRP Reinforcement) limits the design strain level in the FRP reinforcement to $\kappa\varepsilon_{Lu} \le 0.90\,\varepsilon_{Lu}$, where,

$$\kappa = 1 - \frac{n E_L t}{428\ \text{kN/mm}} \quad \text{for} \quad n E_{,,} t \le 210\ \text{kN/mm} \quad \text{or}$$

$$\kappa = \frac{105\ \text{kN/mm}}{n E_L t} \quad \text{for} \quad n E_L t > 210\ \text{kN/mm}.$$

n is thenumber of plies, and κ is a strain limit factor for the FRP laminate.

$\kappa = 1 - \frac{1 \times 155 \times 1.2}{428} = \frac{186}{428} = 0.565$ and $\kappa\varepsilon_{Lu} = 0.565 \times 1.9\% = 1.07\%$ for the FRP laminate used here. In the case of the beams tested here, the design strain level would thus be 57 % of the FRP ultimate tensile strain. Table 6a and Fig. 31 (Proposal 1) show that this strain was close to being achieved in beams 4a and 4b, where sufficient anchorage was provided, e.g., by clamping or wrapping with multiple layers of FRP fabric. For beam 4b, the six layers of end wrap probably would have achieved this level of strain, had the concrete not crushed first. However, beams 5 **and** 6 did not come close to achieving this FRP strain, in spite of end clamps or wraps, and failed by FRP debond or interlaminar slip.

Anchorage: The level of strain achieved here in the FRP at midspan corresponds to a load greater than the anchorage capacity that can be achieved by bond only. Using **Eq.** (1) and (2) and $f_{cube} = 1.25\, f_c = 52.5$ MPa, one obtains $f_t = 2.52$ MPa, $l_{max} = 190$ mm, $T_{max} = 22.1$ kN $= 0.153\, F_{Lu}$ for $w = 50$ mm, and $T_{max} = 37.7$ kN $= 0.131\, F_{Lu}$ for $w = 100$ mm (beam 4b). The design values of T_{max} are conservative and are lower than 95 % of Neubauer and Rostasy's measurements (1997). The best fit to their data is obtained if the coefficient of 0.5 in Eq. (1) is changed to 0.64 in the expression for T_{max} (Rostasy, 1998), giving $T_{max} = 28.3$ kN $= 0.197\, F_{Lu}$ for w = 50 mm, and $T_{max} = 48.3$ kN $= 0.168\, F_{Lu}$ for w = 100 mm. Fig. 31 shows the anchorage capacity in terms of strains.

For comparison, values between 32 % and 53 % of FRP ultimate strain were achieved at midspan for $w = 50$ mm, and 52 % of ultimate strain was achieved for $w = 100$ mm (Table 6a). Mechanical clamping and adhesion anchored the laminate in beam 4a to a strain of 1.01 % (53 % of rupture), whereas a diagonal wrap with six layers anchored the carbon laminate in beam 4b to a strain of 0.988 %, (52 % of rupture), without slip. Since beam 4b failed by concrete crushing, it is not known how much more effective this wrap would have been. **A** transverse wrap with two layers (beam 5), however, failed at a laminate strain of 0.662 % (35 % of rupture).

It should be noted that Neubauer and Rostasy measured anchorage capacity by double shear, push-out tests, whereas the force required to anchor the ends of the FRP laminate in a four-point bending test is lower than the maximum tension at midspan, depending on how much of the laminate has debonded in the shear span. Since the present experiments show significant debonding in the shear span, usually initiating at the flexural-shear cracks below the load points, the data indicate that clamping or wrapping combined with adhesion can double or triple the anchorage capacity that can be expected from bond only. This agrees with the results of Jensen et al. (1999), who showed that the addition of transverse strips enhances the anchorage capacity from 30 kN to 45 kN. They also showed that clamping produced by three or more steel plates and bolts that do not puncture the carbon strips enhances the ultimate anchorage capacity from 30 kN to 90 kN.

Ductility: The curvature at ultimate load of beams reinforced with steel and carbon FRP varies between 1.43 and 1.86 times that of a beam with a steel reinforcement ratio of 75 % of the balanced ratio (maximum allowed by **ACI,** Fig. 30). Thus, beams reinforced with steel and carbon FRP have adequate deformation capacity in spite of their brittle failure modes (concrete crushing, laminate debonding or delamination).

The Canadian Highway Bridge Design Code (CHBDC 2000) ductility criterion is reasonable (Fig. 30). All the beams (4b, 7N and 8N) that failed by concrete crushing fulfilled the criterion, whereas the beams that failed by debond or delamination did not (beams 4a, 5 and 6). Beam 9, which is a normal RC beam with no external FRP strengthening, falls slightly short of the criterion. Fig. 25 shows, however, that beam 9 resists moments only slightly less than the peak moment at curvatures much greater than that which corresponds to the peak moment. **A** more relaxed interpretation of the moment-curvature data, obtained by taking ultimate at concrete crushing, would make beam 9 satisfy the criterion.

Results (Table 6a) show that Naaman et al.'s recommendation (1999) to allow an increase in moment due to strengthening up to 20 % of the moment of beam 10, which has the maximum reinforcement ratio allowed by ACI, is reasonable (Fig. ***32)***. Only in beam 4b, which has very low steel and very high carbon reinforcement ratios, does strengthening produce an increase in moment greater than 0.20 **x** ***252*** kN·m = 50.4 kN·m. Beam 4a is at the limit of the recommended allowable moment increase, and all the other strengthened beams would satisfy the criterion. Some of the beams tested, however, did not fail by concrete crushing, and their flexural capacity with proper FRP anchorage is not known from this study.

5. Conclusions

1. The application of carbon FRP laminates is very effective for flexural strengthening of reinforced concrete beams, provided proper anchorage of the laminate is ensured. As the amount of steel reinforcement increases, the additional strength provided by the carbon FRP external reinforcement decreases.

2. Mechanical clamping or wrapping with FRP fabric combined with adhesion is effective in anchoring the FRP laminate and increases the anchorage capacity above that expected for adhesive bond only.

3. If proper anchorage is provided, such as by wrapping or clamping, the effective strain limit (or stress level) currently proposed informally for FRP reinforcement by ACI 440 is close to being achievable for this particular type of carbon FRP. For lightly (steel) reinforced beams, this design stress level in the FRP can add substantially and economically to the beam strength.

4. The curvature at ultimate load of beams reinforced with steel and carbon FRP varies between 1.43 and 1.86 times that of a beam with a steel reinforcement ratio of 75 % of the balanced ratio (maximum allowed by ACI). Thus, beams reinforced with steel and carbon FRP have adequate deformation capacity in spite of their brittle failure modes (concrete crushing, laminate debonding or delamination).

5. The Canadian Highway Bridge Design Code (CHBDC 2000) ductility criterion is reasonable. All the beams (4b, 7N and 8N) that failed by concrete crushing fulfilled the criterion, whereas the beams that failed by debond or delamination did not (beams 4a, 5 and 6).

6. Naaman et al.'s recommendation (1999) to allow an increase in moment due to strengthening up to 20 % of the moment of beam 10, which has the maximum reinforcement ratio allowed by ACI, is reasonable.

7. A proper design procedure for FRP external strengthening should take into account enhancement of FRP anchorage by mechanical clamping, wrapping with FRP fabric, or other means. With that knowledge, and the existing anchorage data (Neubauer and Rostasy 1997), rational and efficient designs are possible.

Notation

a	distance from compression extreme fiber to center of compression
A_L	cross sectional area of carbon FRP laminate
A_s	area of steel flexural reinforcement
b	beam width
c	compression depth
d	beam depth
E_L	laminate modulus of elasticity
E_s	steel modulus of elasticity
F_c	concrete force
F_L	laminate force
F_s	steel force
f_c	concrete cylinder compressive strength
f_{cube}	concrete cube compressive strength
f_{Lu}	ultimate laminate strength
f_t	concrete surface pull-off strength
f_y	yield strength of steel flexural reinforcement
h	beam height
l_{max}	anchorage length needed to develop T_{max}
M	moment
M_R	moment at application of FRP laminate
M_u	measured ultimate moment of tested beam
M_V	calculated ultimate moment of virgin beam
$M_{.001}$	beam moment at a concrete maximum compressive strain of 0.001
n	number of plies
r	radius of curvature
t	laminate thickness
T_{max}	capacity of adhesively bonded anchorage
w	laminate width
y	location measured from the neutral axis ($0 \le y \le c$)
ε_0	strain at which concrete attains its compressive strength (= 0.0025)
ε_i	tensile strain on concrete surface at application of FRP laminate
ε_c	concrete compressive strain
ε_{cM}	compressive strain on concrete extreme fiber
ε_{cu}	concrete ultimate strain (= 0.003)
ε_h	tensile strain on concrete extreme fiber
ε_L	laminate strain
ε_{LM}	maximum laminate strain (at beam failure)
ε_{Lu}	laminate rupture strain
ε_s	steel strain
κ	FRP strain limit factor
ρ_b	balance ratio of steel flexural reinforcement
ρ_s	ratio of steel flexural reinforcement
σ_c	concrete compressive stress
ϕ	beam curvature

ϕ_u ultimate curvature of tested beam
ϕ_V calculated ultimate curvature of virgin steel RC beam
ϕ_{Vb} calculated ultimate curvature of RC beam with 75 % of balanced steel ratio
$\phi_{.001}$ beam curvature at a concrete maximum compressive strain of 0.001

References

American Concrete Institute (1999), "Building Code Requirements for Structural Concrete," ACI 318-99.

Aprile, A., Limkatanyu, **S.** and Spacone, E. (2001), "Analysis of RC Beams with FRP Plates", ASCE Structures Congress, Washington D.C.

Bonacci, J.F. (1996), "Strength, Failure Mode and Deformability of Concrete Beams Strengthened Externally with Advanced Composites," Proceedings of the 2nd International Symposium on Advanced Composite Materials in Bridges and Structures, Montreal, Canada, pp. 419-426.

Canadian Standards Association (2000), Canadian Highway Bridge Design Code, Section 16, "Fibre-Reinforced Structures", Rexdale, Ontario.

Concrete Society (2000), "Design Guidance for Strengthening Concrete Structures Using FRP Composite Materials", Technical Report No. 55, Crowthome, Berkshire, UK.

German Institute of Construction Technology (1997), "Strengthening of Reinforced Concrete and Prestressed Concrete with Sika Carbodur Bonded Carbon Fiber Plates", Authorization No. 2-36.12-29, Berlin.

Jaeger, L.G., Mufti, **A.A.** and Tadros, G. (1997), "The Concept of the Overall Performance Factor in Rectangular Section Reinforced Concrete Members", Proc. 3rd Int. Symp. on *Non-Metallic (FRP)Reinforcementfor Concrete Structures*, Sapporo, Japan, Vol. 2, pp. 551-559.

Japan Building Disaster Prevention Association (JBDPA, 1999), "Seismic Retrofitting Design and Construction Guidelines for Existing RC Buildings with FRP Materials".

Jensen, A.P., Petersen, C.G., Poulsen, E., Ottosen, C. and Thorsen, T. (1999), "On the Anchorage to Concrete of Sika CarboDur CFRP Strips", Int. Congress: *Creating with Concrete*, Dundee, Scotland.

Meier, U. (1987), "Bridge Repair with High Performance Composite Materials", *Material und Technik*, Vol. 15, pp. 125-128.

Naaman, **A.E., Park, S.Y.,** Lopez, M.M., and Till, R.D. (2001), "Parameters Influencing the Flexural Response of RC Beams Strengthened Using CFRP Sheets", *FRPRCS-5*, University of Cambridge, UK, pp. 117-125.

Naaman, **A.E.,** Park, S.Y., Lopez, M.M., Stankiewicz, and Pinkerton, L. (1999), "Repair and Strenthening fo RC Beams Using CFRP Laminates", University of Michigan Reports No. UMCEE 99-04, 97-12, 98-21, 98-38, 98-39, Ann Arbor, MI.

Neubauer, U. and Rostasy, F.S. (1997), "Design Aspects of Concrete Structures Strengthened with Externally Bonded CFRP Plates", Concrete and Composites, Proc. 7th Int. Conf. on *Structural Faults and Repair,* Vol. *2,* pp. 109-118, ECS Pub. Edinburgh, Scotland.

Rostasy, F.S. (1998), "Assessment of S&P CRP Structural Strengthening System", Expert Opinion No. 98/0322, Scherer & Partners Construction System, Brunnen, Switzerland.

Smith, **S.T.** and Teng, J.G. (2001), "Strength Models for Plate End Debonding in FRP – Strengthened RC Beams", *FRPRCS-5*, University of Cambridge, UK, **pp.** 419-428.

Swamy, R.N. and Mukhopadhyaya (1999), "Debonding of Carbon-Fibre-Reinforced Polymer Plate from Concrete Beams', Proc. Instn. Civil Engineers, *Structures and Buildings,* Vol. 134, Nov., pp. 301-317.

Triantafillou, T., Matthys, S., and Taerwe, L. (2001), " Design of Concrete Members Strengthened with Externally Bonded FRP Reinforcement", *FRPRCS-5*, University of Cambridge, UK, pp. 157-166.

Acknowledgments

The authors thank Frank Davis for overall technical assistance with the tests, and Fahim Sadek, Joannie Chin and especially Nicholas Carino for their critical review of a first draft of this paper. The authors are also grateful to the SIKA Corporation for supplying Carbodur laminates, Sikadur **30** adhesive, Sikawrap Hex 230C and Sikadur 330 impregnating resin. The material properties used in this work reflect manufacturer's published data at the time.

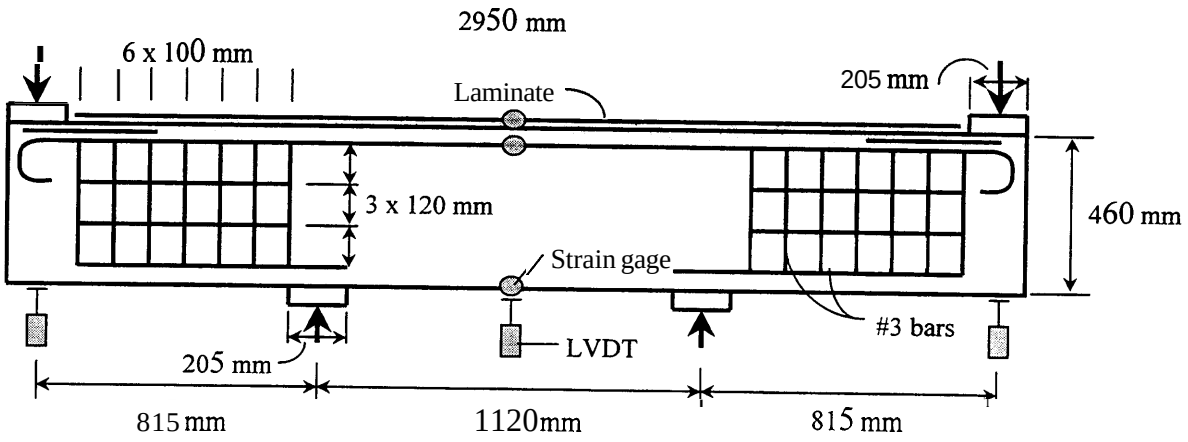

Fig. 1 Beam reinforcement and test set-up

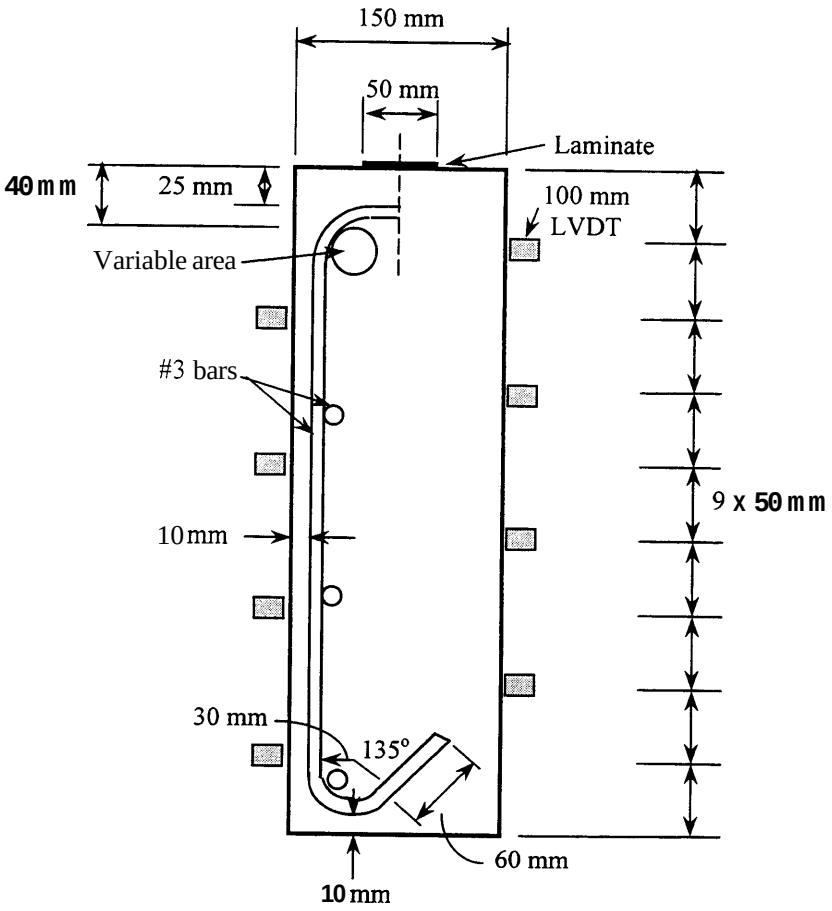

Fig. 2 Beam cross-section showing stirrups at shear span and LVDTs at midspan

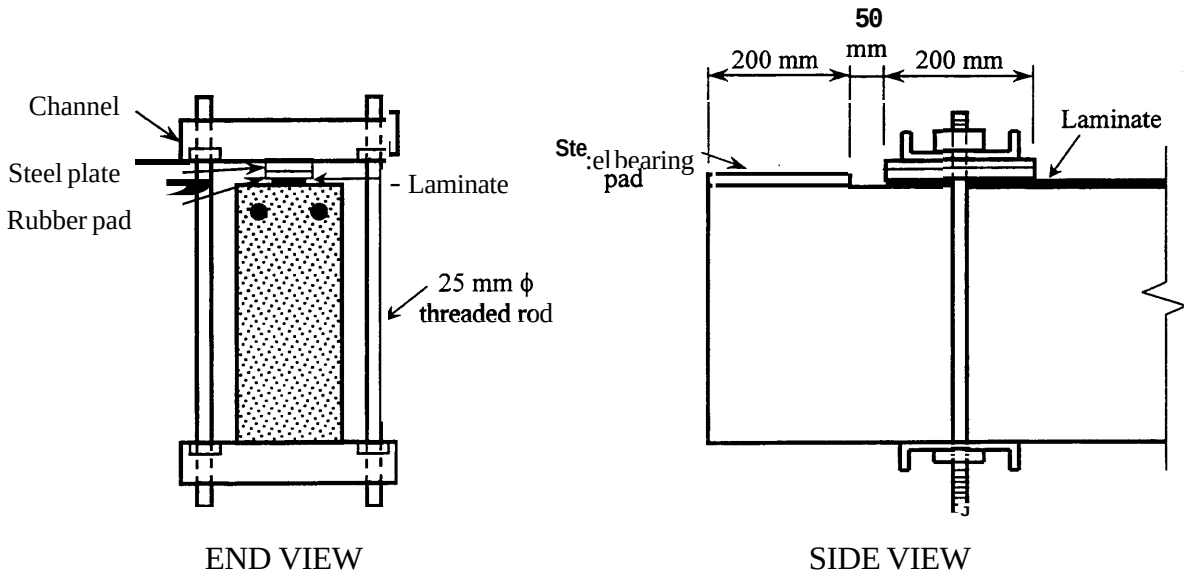

Fig. 3 Clamping of ends of laminate

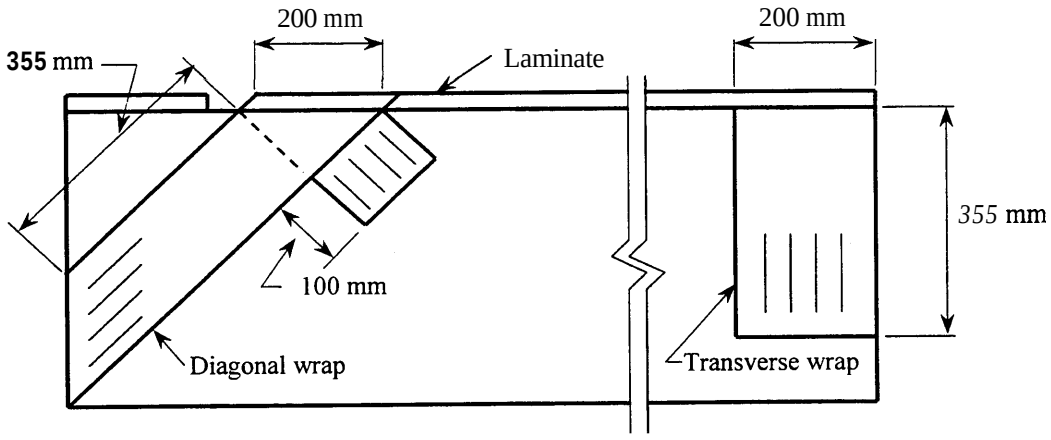

Fig. 4 End **wraps** using carbon fiber fabric

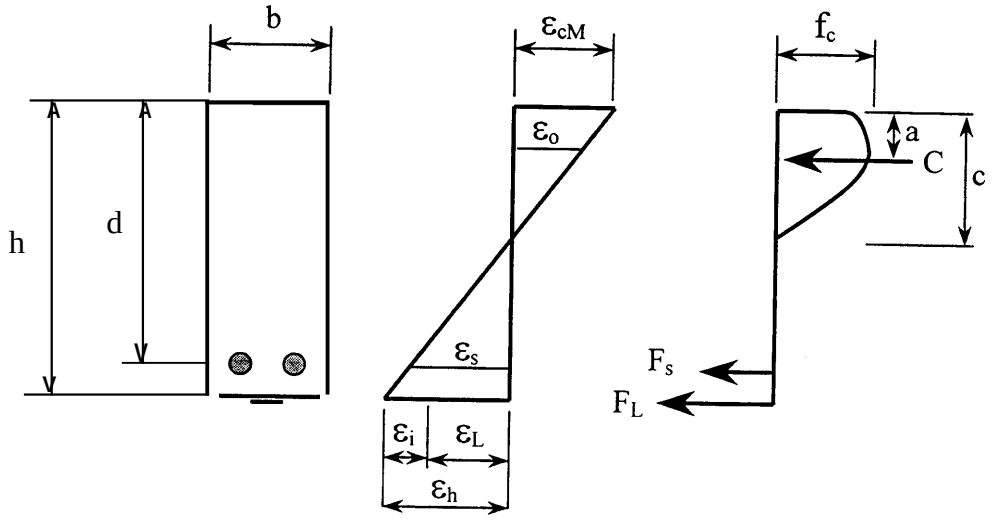

Fig. 5 Beam stresses and strains

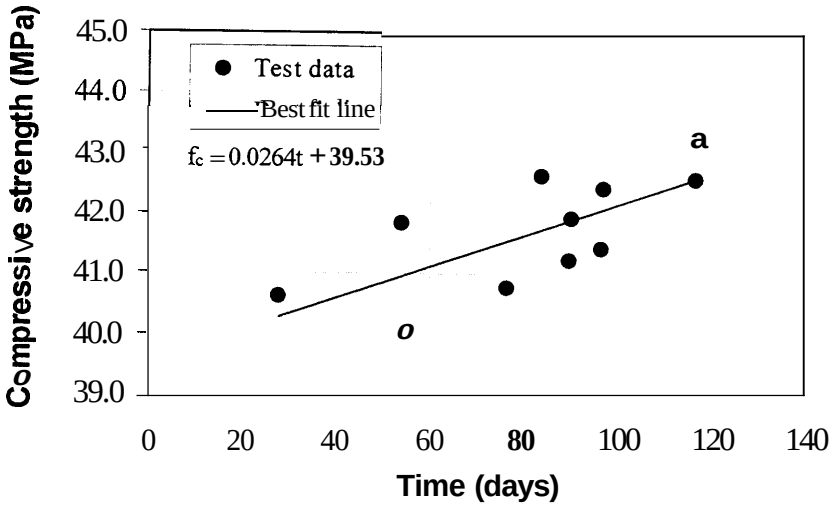

Fig. 6 Compressive strength of concrete

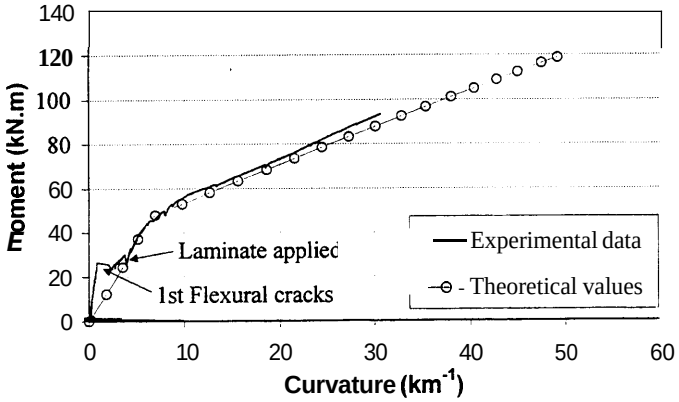

Fig. **7** Curvature vs. moment (beam 4a)

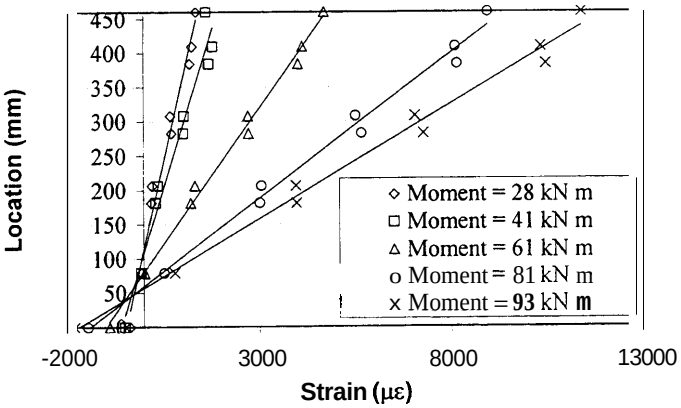

Fig. **8** Strain profiles (beam 4a)

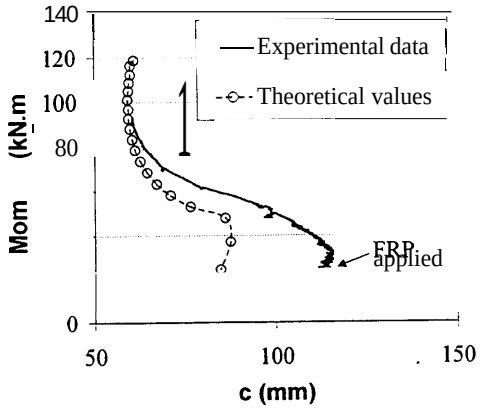

Fig. **9** Compression depth vs. moment (beam 4a)

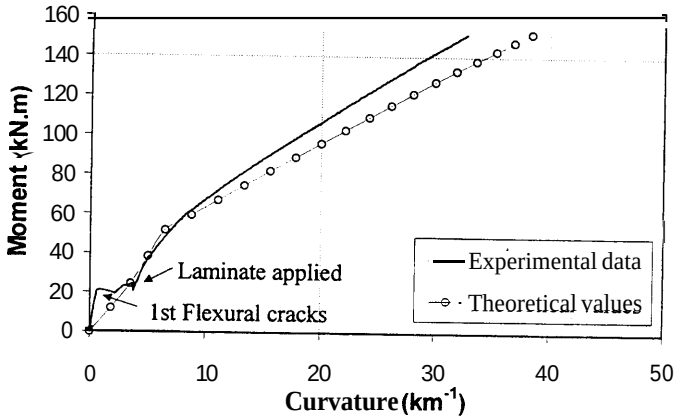

Fig. 10 Curvature vs. moment (beam 4b)

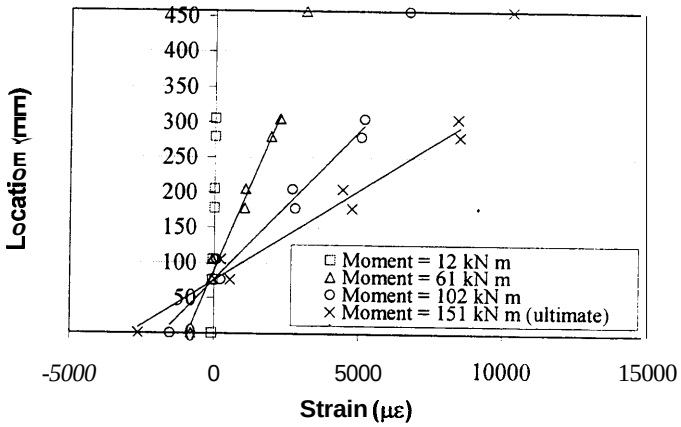

Fig. 11 Strain profiles (beam 4b)

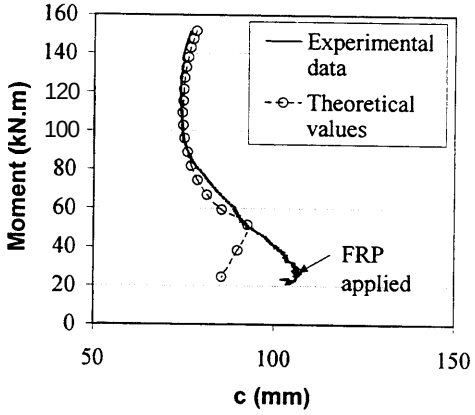

Fig. 12 Compression depth **vs.** moment (beam 4b)

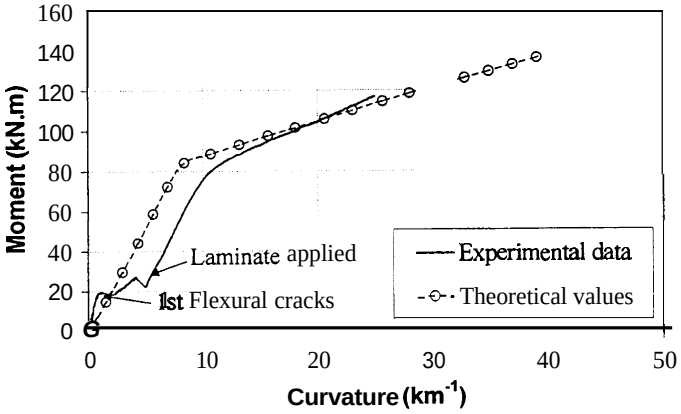

Fig. 13 Curvature vs. moment (beam 5)

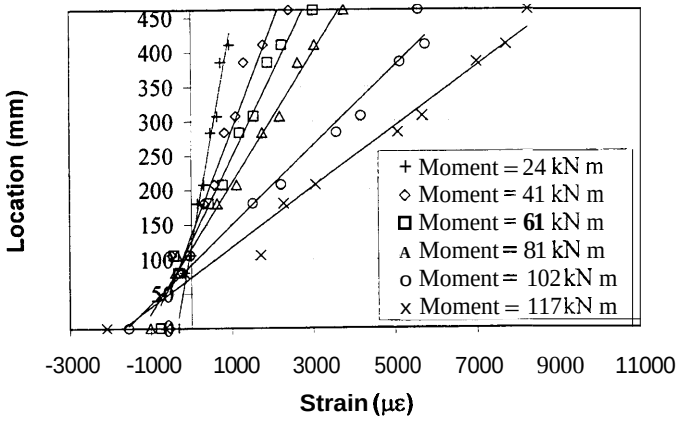

Fig. 14 Strain profiles (beam 5)

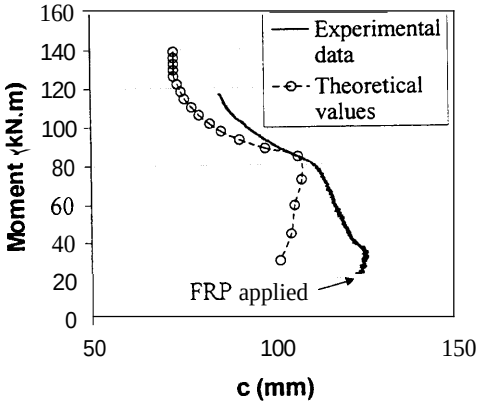

Fig. 15 Compression depth vs. moment (beam 5)

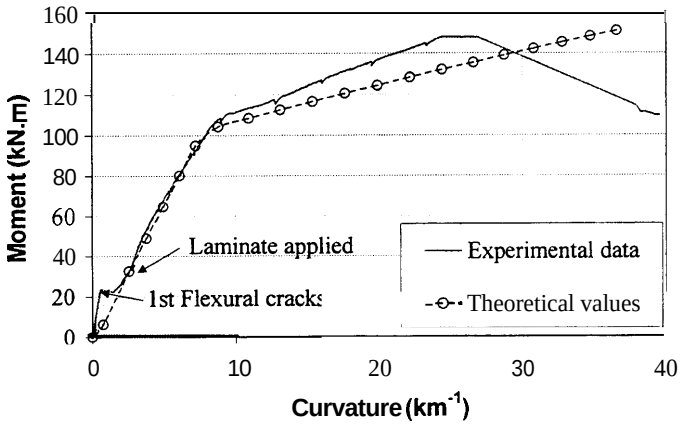

Fig. 16 Curvature vs. moment (beam 6)

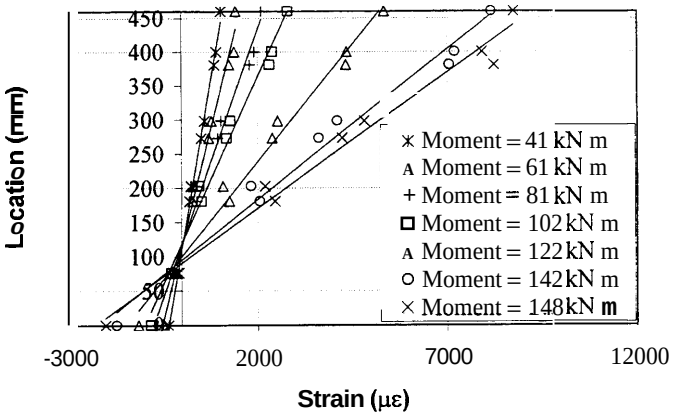

Fig;. 17 Strain profiles (beam 6)

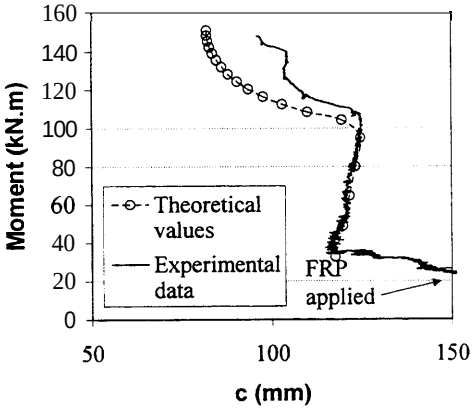

Fig. **18** Compression depth vs. moment (beam 6)

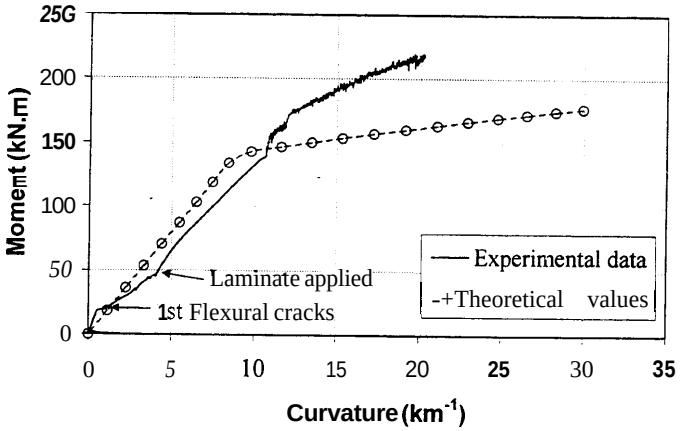

Fig. 19 Curvature vs. moment (beam 7N)

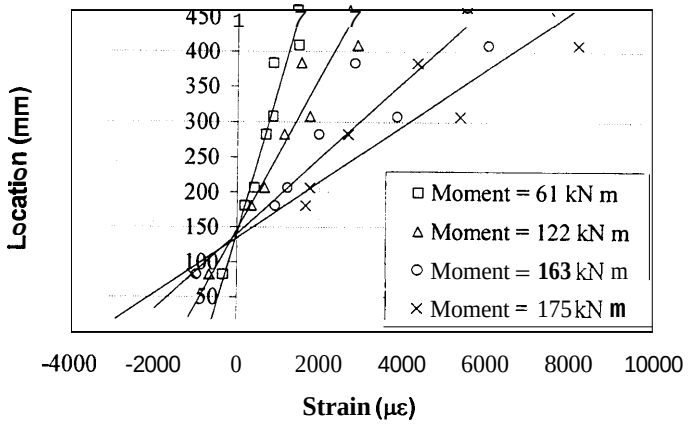

Fig. 20 Strain profiles (beam 7N)

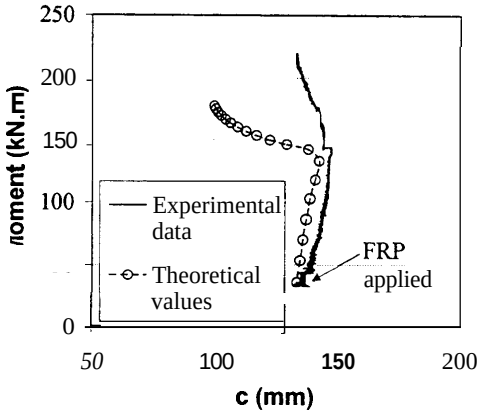

Fig. 21 Compression depth **vs.** moment (beam 7N)

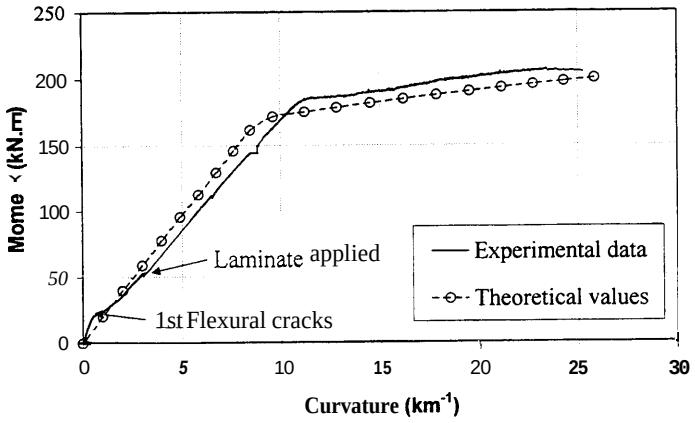

Fig. 22 Curvature vs. moment (beam 8N)

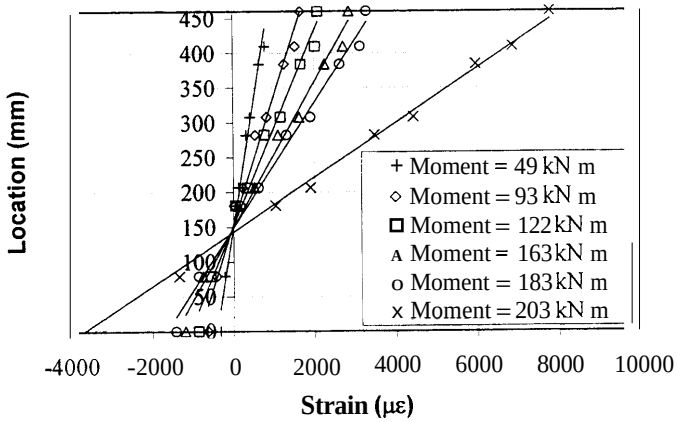

Fig. 23 Strain profiles (beam 8N)

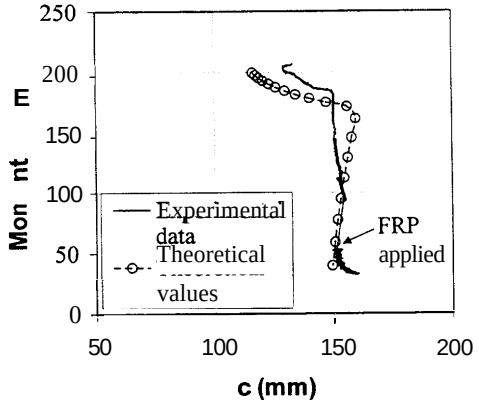

Fig. 24 Compression depth vs. moment (beam **8N)**

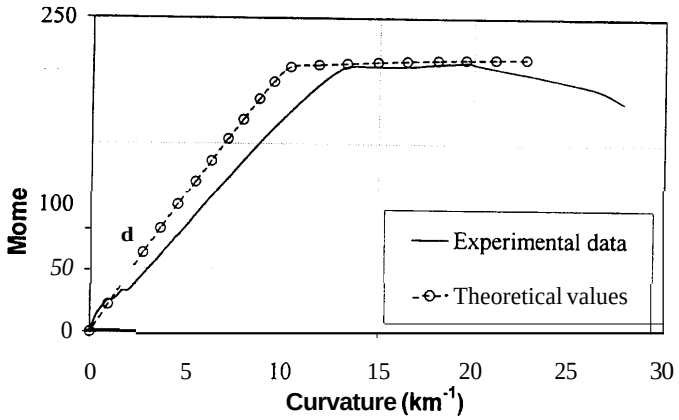

Fig. 25 Curvature vs. moment (beam 9)

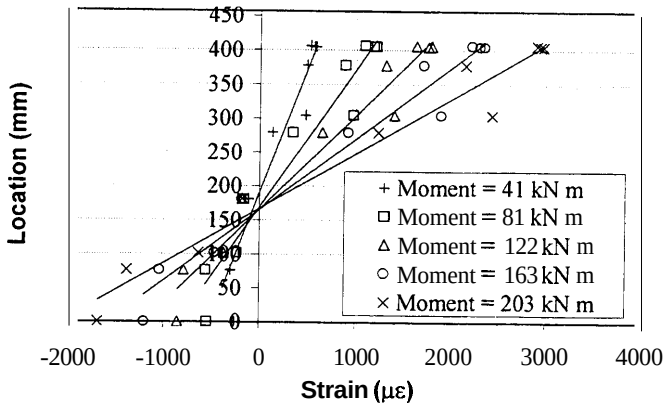

Fig. 26 Strain profiles (beam 9)

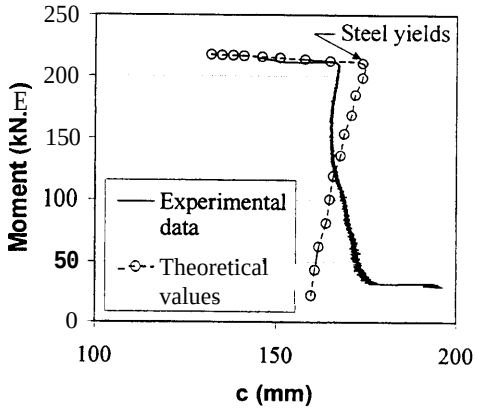

Fig. 27 Compression depth vs. moment (beam 9)

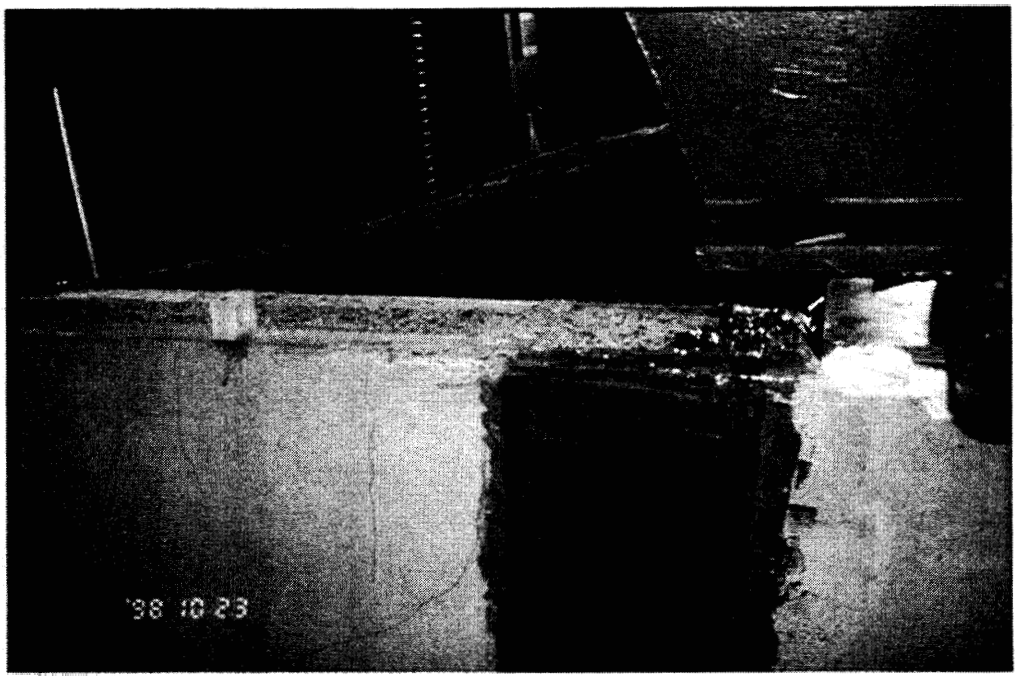

Fig. 28 Failure of **transverse wrap and debonding of laminate (Beam** *5)*

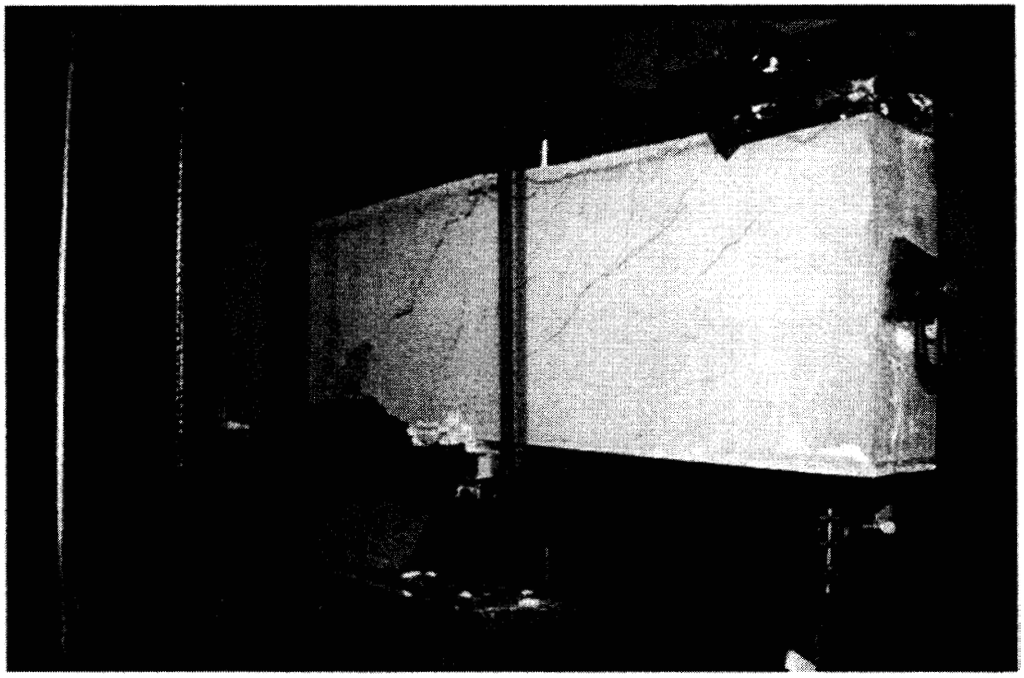

Fig. 29 Flexural and shear cracks. Compression failure (Beam *6)*

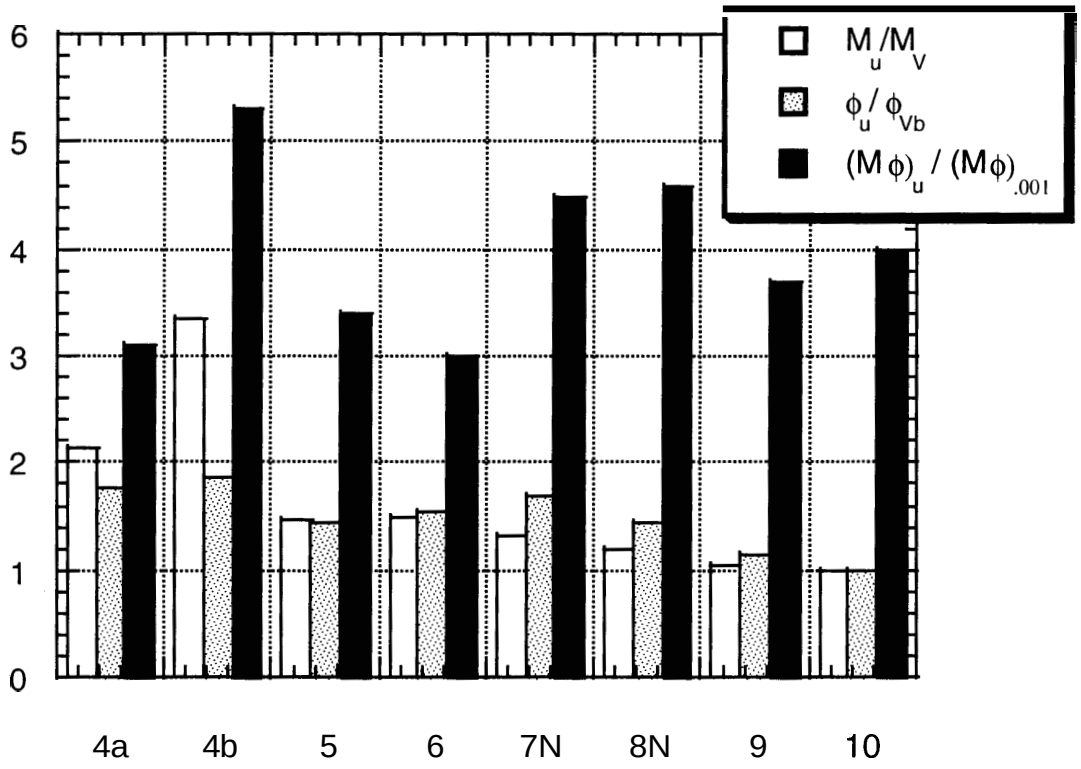

Fig. 30 Moment and curvature ratios

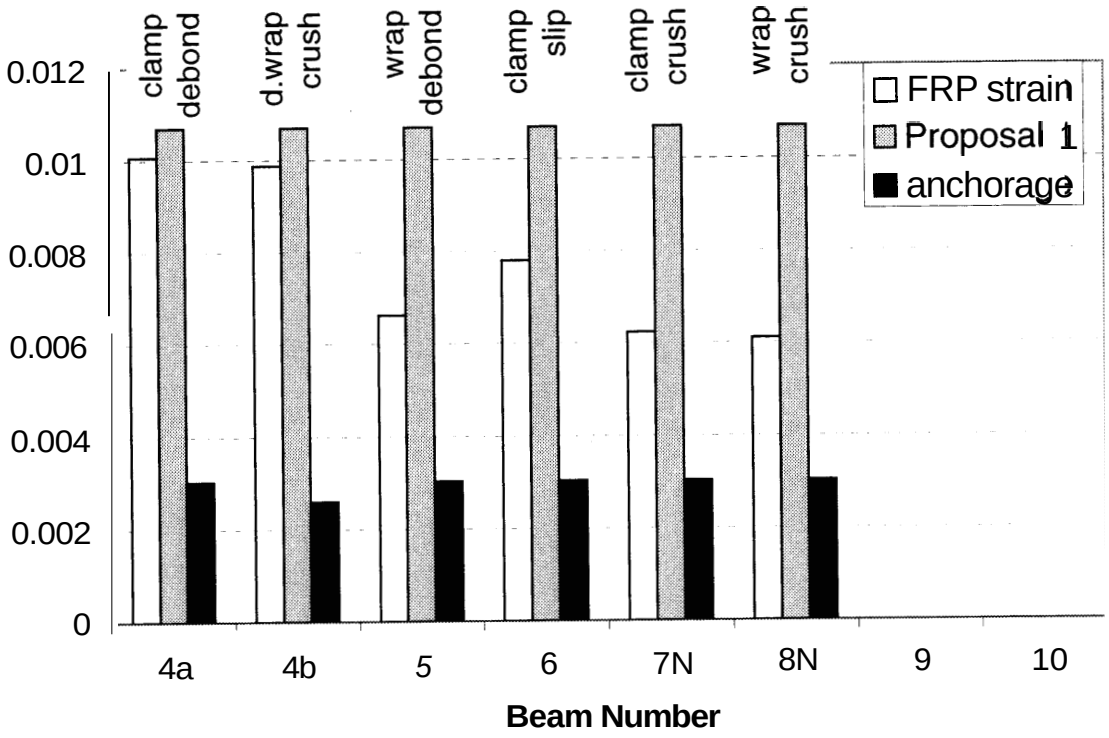

Fig.31 Measured FRP strain, calculated anchorage capacity and a proposed FRP limit strain

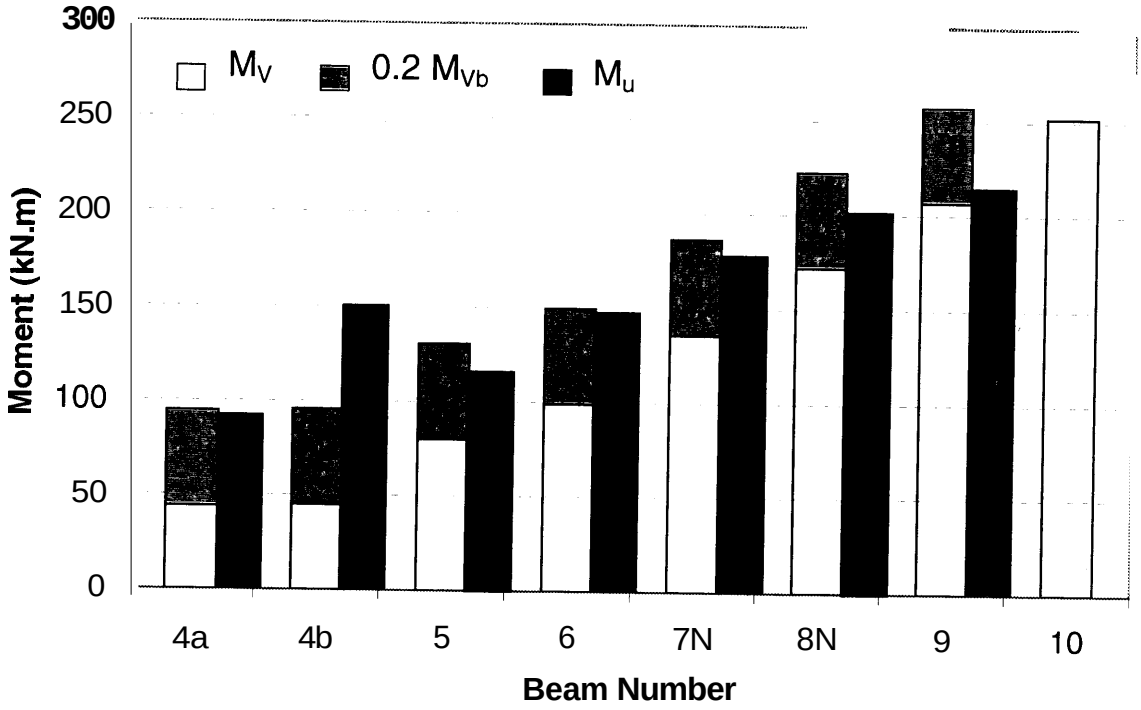

Fig.32 Moment increase and **a** proposed strengthening limit